Regular paper

Microstrip Bandpass Filters using Coupled Feed Lines for Third and Fourth Generation Communications

Amirhossein Ghaderi, Alireza Golestanifar, Farzin Shama

PII: S1434-8411(17)32934-5
DOI: https://doi.org/10.1016/j.aeue.2018.02.007
Reference: AEUE 52234

To appear in: *International Journal of Electronics and Communications*

Received Date: 14 December 2017
Accepted Date: 2 February 2018

Please cite this article as: A. Ghaderi, A. Golestanifar, F. Shama, Microstrip Bandpass Filters using Coupled Feed Lines for Third and Fourth Generation Communications, *International Journal of Electronics and Communications* (2018), doi: https://doi.org/10.1016/j.aeue.2018.02.007

Microstrip Bandpass Filters using Coupled Feed Lines for Third and Fourth Generation Communications

Amirhossein Ghaderi[1], Alireza Golestanifar[1*], Farzin Shama[2]

[1]Young Researchers and Elite Club, Kermanshah Branch, Islamic Azad University, Kermanshah, Iran

[2]Department of Electrical Engineering, Kermanshah Branch, Islamic Azad University, Kermanshah, Iran

Emails: Amir92h@yahoo.com, Golestany950@yahoo.com, f.shama@aut.ac.ir

[*]Corresponding author (Email: Golestany950@yahoo.com, Tel: +989374158884)

Microstrip Bandpass Filters using Coupled Feed Lines for Third and Fourth Generation Communications

Abstract: In this paper, two compact tuneable bandpass filters (BPFs) based on the coupled feed lines are introduced. To approach a compact size, the coupled feed lines are bended. To design a high performance single-band bandpass filter (BPF), coupled feed lines are loaded by T-shaped stubs (as main resonators) and rectangular stubs (as suppressor stubs). Also, the mechanism of coupled feed lines combining with T-shaped open stubs is analyzed to show a tunable passband. The dual-band BPF includes two big radial-stubs, two small radial-stubs, two T-shaped structures and spiral coupled feed lines. The LC model of big radial-stubs is analyzed to compute the equation of transmission zero using its transfer function. The passband frequency of single-band BPF resonates at 2.12 GHz (3G) with corresponded insertion loss of 0.83 dB. Also, for dual-band BPF, the measured insertion-losses of first and second passbands are close to 0.8 and 1.1 dB, respectively. The frequency responses of BPFs are easily adjusted by altering the physical dimensions, demonstrating a adjustable performance. To verify the correct operation of circuits, the proffered filters are implemented and tested.

Keywords: Bandpass filters, Dual-band, Radial-stub, Single-band, T-shaped, Tuneable.

1 INTRODUCTION

Bandwidth selection is one of the important issues in modern communication systems and the BPFs has significant place in this case. Today, single-band and dual-band operators have been so prevalent in wireless communication. The advantages of a BPF can be expressed as: compact circuit size, good isolation between passbands, high selectivity, and wide stopband [1]. The presented BPFs in [2–30] have been designed using the various configurations, such as stepped-impedance structures, open-circuited stubs, T-shaped resonators, substrate integrated waveguide (SIW) technology, balance differential topology, dual-layer structures and coupled lines that the specifications of each of them are briefly investigated. In [2], a simple structure dual-band bandpass filter has been introduced with compact dimensions. But in this design, the circuit presents a weak harmonic suppression in upper stopband. A compact size dual-band BPF has been fabricated in [3], using stepped-impedance units as resonators, which cannot provides a wide stopband. In [4], single and dual-band BPFs with coupled lines and a large circuit area have been designed. This dual-band BPF can be applied at WLAN and WiMAX. Using the short/open ended stubs two dual-band BPFs with good isolation between the passbands have been designed and implemented in [5]. Nevertheless, the dimensions of these BPFs are suitable; insertion losses of passbands are high. The presented BPF in [6] has been implemented using coupled lines with operational frequencies of 1.57 and 2.45 GHz. The benefit of this filter is compact physical dimensions, although it deactivate only up to 3rd harmonics. Generally, wide-band BPFs cannot provide an strong harmonic rejection and sharp attenuation near their passbands [7]. By adopting the interdigital structures as fundamental resonators, BPFs with small size have been fabricated in [8] that both of the complexity of design and analysis are considered as challenges of these circuits. The presented BPFs in [9-10] have been designed by coupling the ring resonators with input/output ports. Large size and high insertion losses of passbands are negative factors of these circuits. Another structure used for designing the BPFs is balance differential topology [11-15]. This structure has a good immunity to interferer and noise and improves the isolation among passbands in dual-band BPF. The coupled structures are widely utilized to design BPFs [16-22]. Compactness and structure simplicity are benefits of this method. Duo to coupling

effects between the lines, the passband width can be regulated to design narrow- and wide-band BPF, as well. Stepped-impedance resonators have been employed in [23-24] to design single- and dual-band BPFs. In [25-26], two dual-band BPFs based on the hybrid structure have been reported that the isolation between the passbands in these circuits is weak. Substrate integrated waveguide technology is another method of filter design [27-28]. The features of this technology include a wide stopband and high sharpness. However, complexity of design and analysis are challenges of this technology. The reported dual-band BPF in [29] suffers from enormous dimensions and narrow stopband width. A multi-layer planar BPF with simple topology has been introduced in [30] that has flat group delay and occupies very small range. Dual-layer and defected coplanar waveguide (CPW) topologies have been applied for designing dual-band BPFs in [31-32]. These circuits provide a good isolation among the passbands; nevertheless deactivation of spurious peaks in the upper stopband is not appropriate. Also, the compact wide-band BPFs in [33-34] have challenges such as weak harmonic elimination in the stopband area.
This paper focuses on the design of applicative, analytical and tuneable BPFs, using the coupled feed lines.

2 DESIGN PROCESS

The design procedure of the single-band and dual-band BPFs are explained below. These structures are implemented based on the coupled feed lines.

2.1 Single-band BPF design

Figure 1 shows the layout of single-band BPF. This circuit is composed of the coupled feed lines, T-shaped resonators and rectangular suppressors. A detailed description of design procedure is presented as follows:

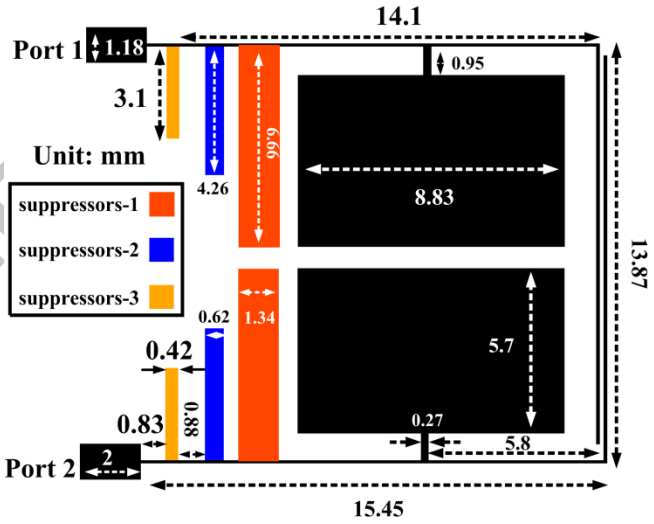

Fig. 1. Layout of single-band BPF.

2.1.1 Coupled feed lines combining with T-shaped open stubs

Narrow-band bandpass filters can be designed using coupled line structures. The equivalent circuit of a coupled line is depicted in Fig. 2. The transmission (ABCD) matrix of this structure is presented in (1), [1].

$$[M]=\begin{bmatrix} \dfrac{Z_{0e}+Z_{0o}}{Z_{0e}-Z_{0o}}\sin\theta\cos\theta & j\dfrac{Z_{0e}-Z_{0o}}{2}\sin^2\theta-\cos^2\theta \\ j\dfrac{2j}{Z_{0e}-Z_{0o}}\sin^2\theta+\cos^2\theta & \dfrac{Z_{0e}+Z_{0o}}{Z_{0e}-Z_{0o}}\sin\theta\cos\theta \end{bmatrix}, \qquad (1)$$

where, Z_{0e} and Z_{0o} are the even and odd mode characteristic impedances of coupled line [1]. $\theta=\beta l$ is the electrical length of line, l is the physical length and the propagation constant is shown by β.

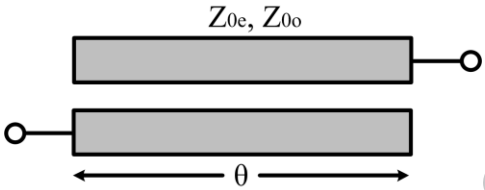

Fig. 2. Equivalent circuit of coupled line, [1].

The dimensions of coupled feed lines are determined to locate the resonance frequency at 2 GHz range. Also, by bending the structure, an excellent compactness is obtained. Next, for achievement a single-band BPF with sharp response and to fix the passband at 2.1 GHz, the coupled feed lines are loaded by two T-shaped open stubs, as depicted in Fig. 3. As seen, these stubs extend the upper stopband up to 6 GHz.

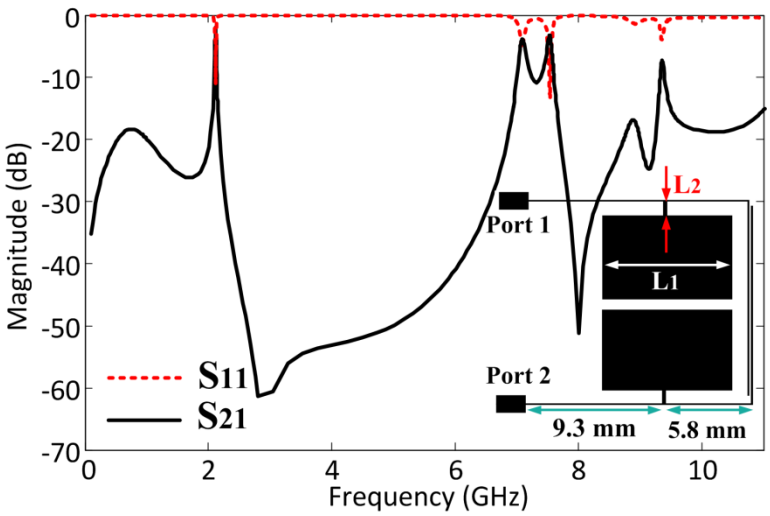

Fig. 3. Layout and EM-simulation of coupled feed lines combining with T-shaped open stubs.

The performance of coupled feed lines combining with T-shaped open stubs is analyzed. The equivalent circuit of this structure is depicted in Fig. 4. In Fig. 4, Z_L, Z_h and Z_0 are the characteristic impedances of low impedance stubs, high impedance stubs and transmission lines, respectively. Z_{inL} and Z_{inh} are the input impedance of low impedance stubs and T-shaped open stubs, respectively. Also, $\theta_1 = \theta_4$, θ_2, θ_3 and θ are the electrical lengths of transmission lines, low impedance stubs, high impedance stubs and coupled lines, respectively.

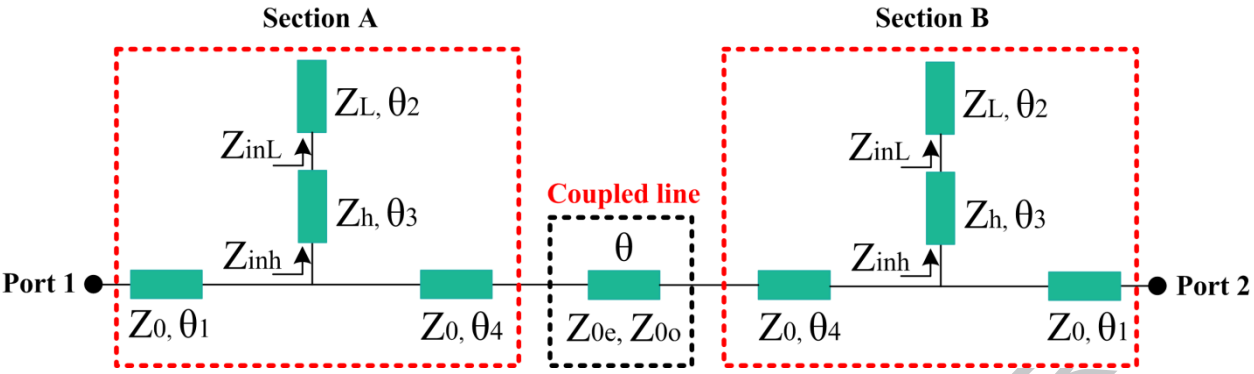

Fig. 4. Equivalent circuit of coupled feed lines combining with T-shaped open stubs.

The ABCD matrix of a transmission line (such as $Z_0/\ \theta_1$) is defined as follows [1]:

$$[T]_1 = \begin{bmatrix} \cos\theta_1 & jZ_0 \sin\theta_1 \\ j\dfrac{1}{Z_0}\sin\theta_1 & \cos\theta_1 \end{bmatrix}. \tag{2}$$

The ABCD matrix for T-shaped loaded open stubs (including Z_L and Z_h) is achieved from [1]:

$$[T]_2 = \begin{bmatrix} 1 & 0 \\ Y_{in_h} & 1 \end{bmatrix}, \tag{3}$$

where:

$$Y_{in_h} = \frac{1}{Z_{in_h}},$$

$$Z_{in_h} = Z_h \times \frac{Z_{in_L} + jZ_h \tan\theta_3}{Z_h + jZ_{in_L} \tan\theta_3},$$

$$Z_{in_L} = -jZ_L \cot\theta_2.$$

Also, another ABCD matrix for transmission line (such as $Z_0/\ \theta_4$) of $[T]_3$ can be similarity defined as follows:

$$[T]_3 = \begin{bmatrix} \cos\theta_4 & jZ_0 \sin\theta_4 \\ j\dfrac{1}{Z_0}\sin\theta_4 & \cos\theta_4 \end{bmatrix}. \tag{4}$$

So, the ABCD matrix of sections A and B can be obtained from:

$$[M]_1 = [T]_1 \times [T]_2 \times [T]_3. \tag{5}$$

$$[M]_2 = [T]_3 \times [T]_2 \times [T]_1. \tag{6}$$

Hence, the total ABCD matrix is obtained as follows:

$$[M]_{total} = [M]_1 \times [M] \times [M]_2. \quad (7)$$

By computing the total ABCD matrix, S_{21}-parameter in terms of ABCD parameters can be written as [1]:

$$S_{21} = \frac{2}{A + B/Z_0 + CZ_0 + D}. \quad (8)$$

According to (8), S_{21}-parameter is related to electrical lengths such as θ_2 ($\theta_2=\beta L_1$) and θ_3 ($\theta_3=\beta L_2$) so that by changing the physical dimensions of T-shaped loaded open stubs (L_1 and L_2), the position of central frequency can be shifted. As seen in Figs. 5 (a) and 5 (b), by reducing the length of L_1 and L_2, the central frequency is shifted to upper frequencies. Hence, the central frequency can be fixed at the desired location by selecting the proper dimensions.

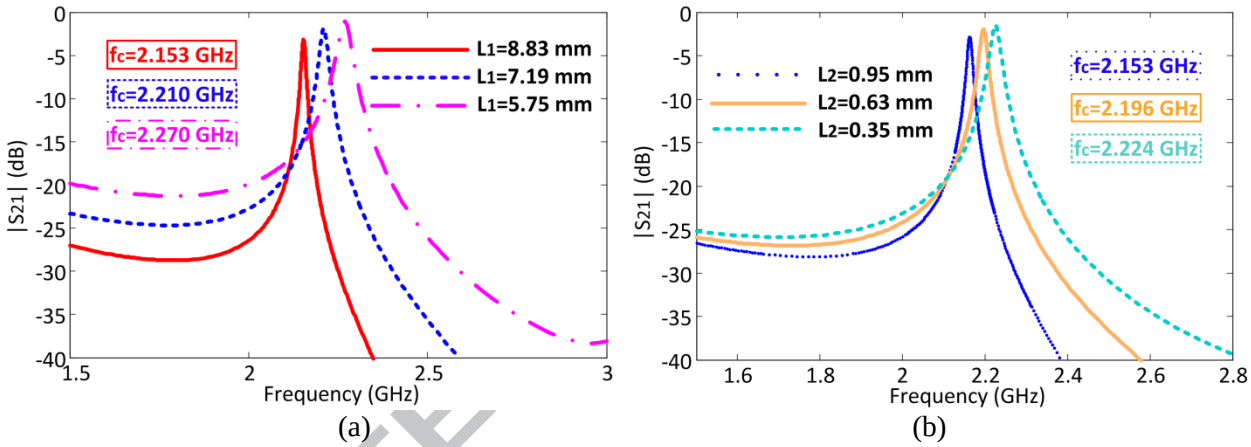

Fig. 5. Coupled feed lines combining with T-shaped open stubs: (a) EM-simulation (S_{21}) with different L_1, (b) EM-simulation (S_{21}) with different L_2.

2.1.2 Suppressors design

Besides, suppressor elements play an important role in designing microstrip filters to reach a wide stopband. For this reason, a pair of suppressors' type 1 (suppressors-1) is presented in Fig. 6. The stopband of the structure is from 6.56 to 9.4 GHz. Also to suppress the spurious peaks in higher frequencies (up to 12.8 GHz), a pair of suppressors' type 2 (suppressors-2) is introduced in Fig. 7. The designed suppressors create some transmission zeros to suppress the unwanted harmonics in stopband range. The frequency of transmission zeros are related to dimensions of open stub. By adjusting the physical dimensions of suppressors, the location of transmission zeros can be fixed to attenuate the spurious peaks.

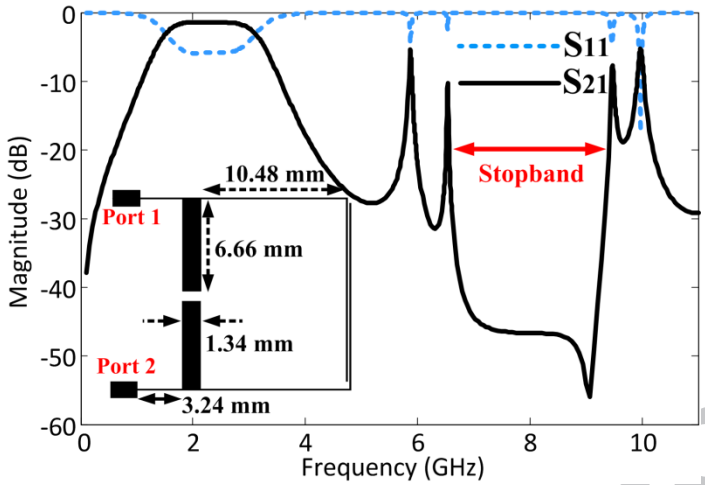

Fig. 6. Layout and EM-simulation of suppressors-1.

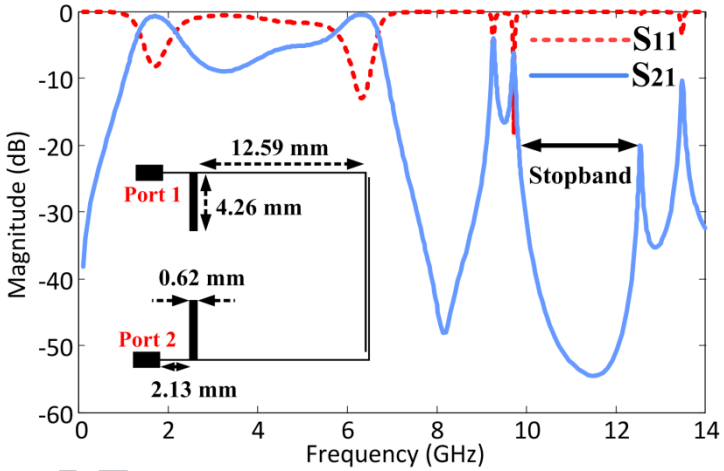

Fig. 7. Layout and EM-simulation of suppressors-2.

2.1.3 BPF design

In order to achieve a wide stopband, the suppressors-1 and suppressors-2 are merged and they are added to couple feed lines combined with T-shaped open stubs. The layout and EM-simulation of fundamental BPF is presented in Fig. 8. As seen, the upper stopband has been increased to 12.8 GHz with -22 dB suppression level. Also, the insertion loss and return loss in passband are 0.96 dB and 13.5 dB, respectively.

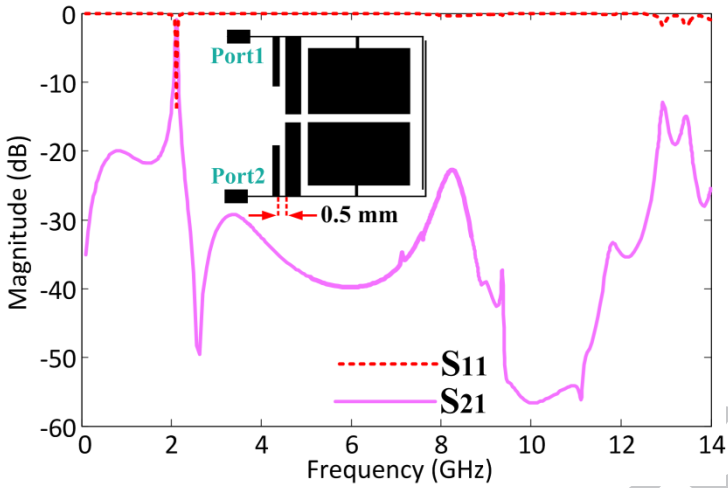

Fig. 8. Layout and EM-simulation of fundamental BPF.

Finally, to design a high performance single-band BPF with remarkable specifications like, high suppression level in stopband area and low insertion loss in passband, a pair of suppressors' type 3 (suppressors-3) is added to fundamental BPF. The manufactured photo, simulation and experimental results of single-band BPF are presented in Fig. 9.

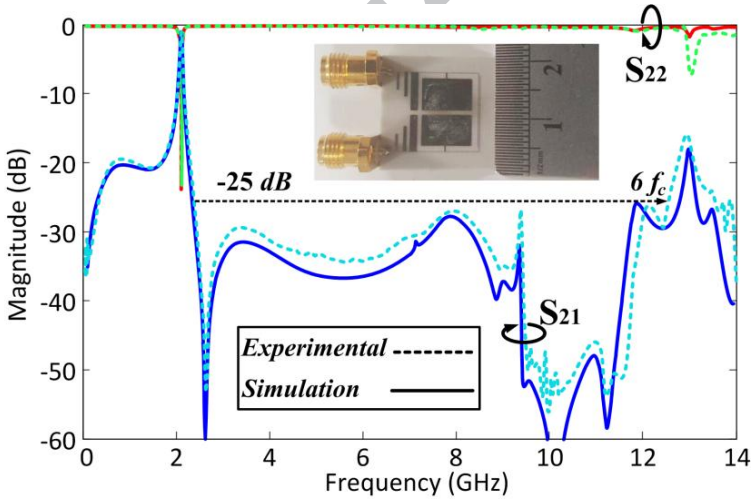

Fig. 9. Photo of manufactured filter, simulation and experimental results of single-band BPF.

As seen in Fig. 10, the single-band BPF has a flexible response so that by tuning the physical lengths of suppressors-3, the suppression level in upper stopband can be easily regulated.

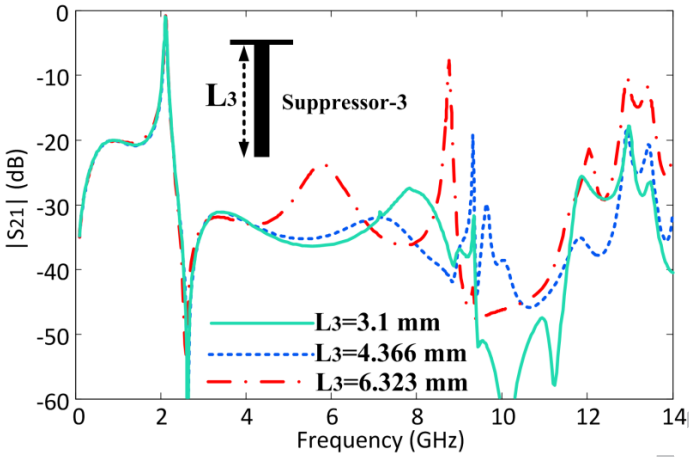

Fig. 10. S_{21} parameter of single-band BPF as a function of different lengths of suppressors-3.

2.2 Dual-band BPF

In this plan, the coupled feed lines are applied to design a dual-band BPF. Figure 11 shows the layout of dual-band BPF. This structure consists of the coupled feed lines; two big radial-stubs (with radiuses of R_1), two T-shaped stubs and two small radial-stubs (with radiuses of R_3). The filter design steps are described.

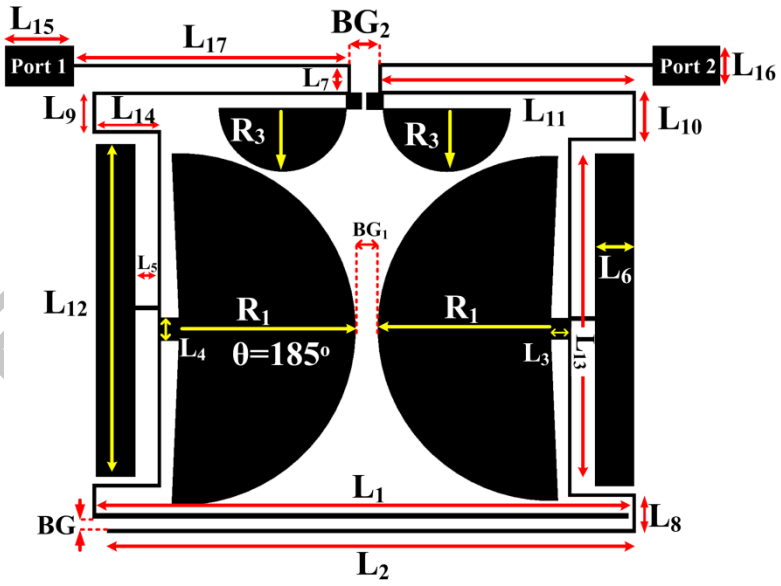

Fig. 11. Layout of Dual-band BPF.

For regulation the passbands at 2.1 and 2.6 GHz frequencies and to provide a wide upper stopband, two big radial-stubs (with radiuses of R_1) are applied. The layout and EM-simulation of structure-1are depicted in Fig. 12(a). Then for suppression the unwanted peaks in the lower stopband, T-shaped stubs are added, as shown in Fig. 12(b). Finally, for improvement the insertion losses and return losses of passbands, two small radial-stubs are utilized. The layout and EM-simulation of dual-band BPF are

exhibited in Fig. 12(c). As seen, the values of insertion losses and return losses in the first and second passbands are 0.81/16.8 dB and 1.13/15.9 dB, respectively.

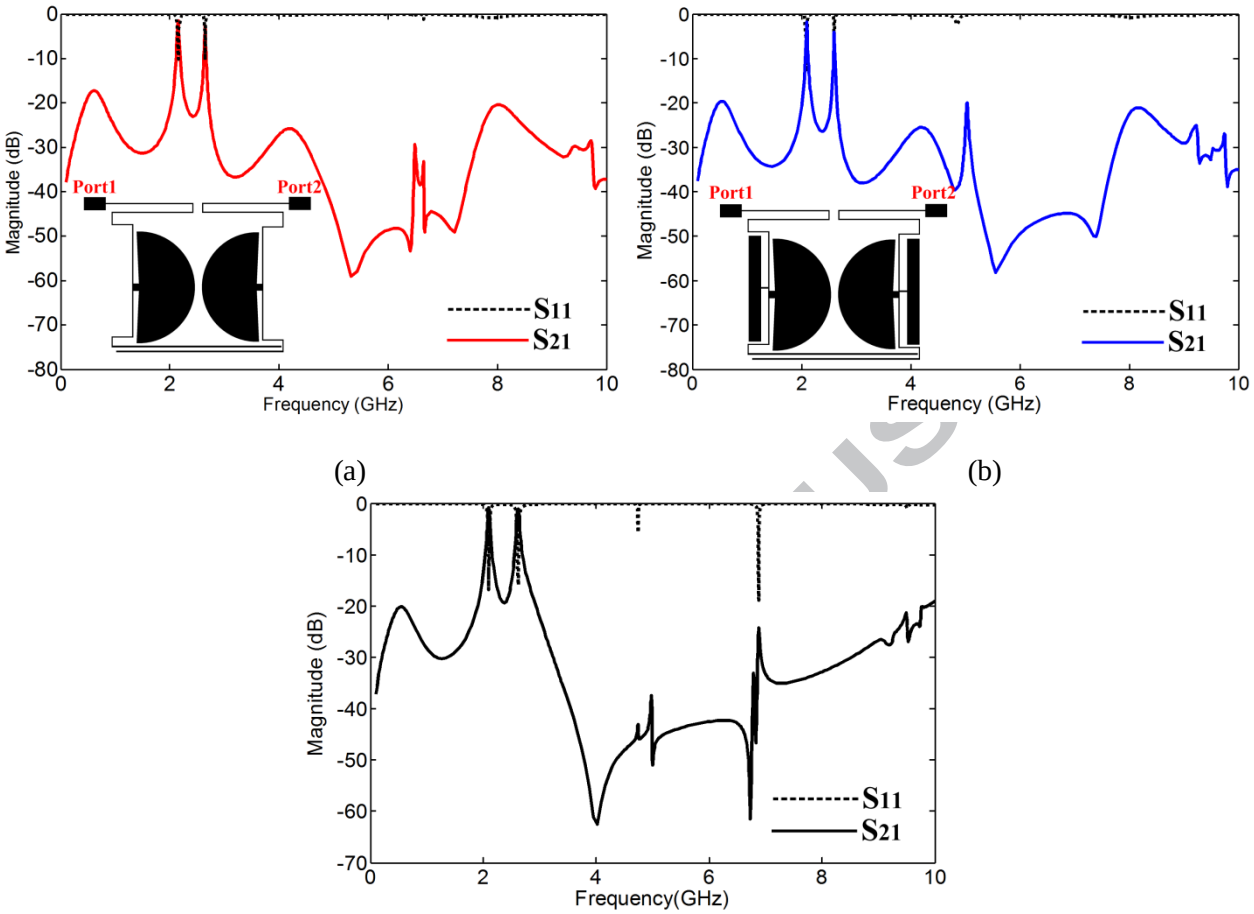

Fig. 12. Layout and EM-simulation: (a) structure-1. (b) structure-2. (c) dual-band BPF.

For the illustrated resonator in Fig. 13(a), the resonator provides a wide rejection band with suitable suppression level. Also, it comprises of a high impedance line, a low impedance stub and one radial stub.

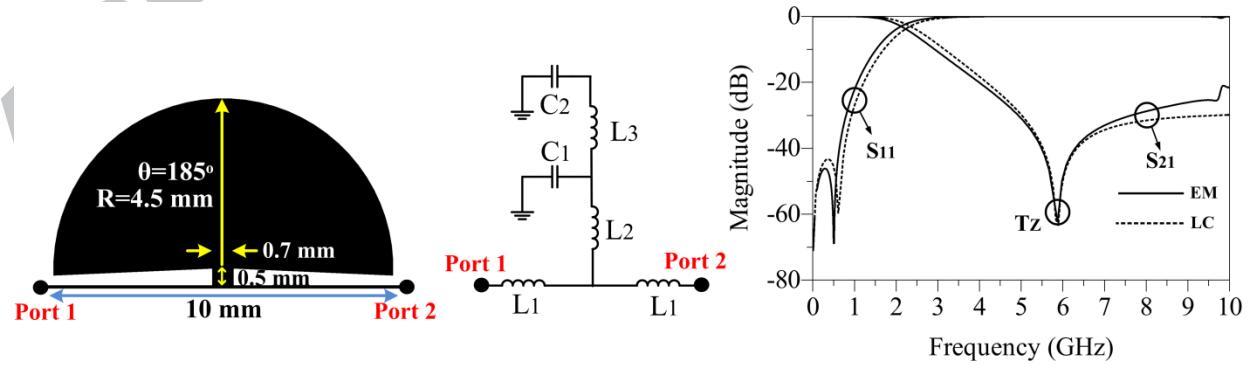

Fig. 13 Big radial-stubs: (a) Layout. (b) LC model. (c) EM and LC simulations.

The radial resonator generates a transmission zero (T_Z) at 5.97 GHz frequency that the stopband width is tuned by it. For analysis the performance of this resonator, an LC model is presented in Fig. 13(b). In this model, L_1 is considered as inductance of high impedance line. L_2 and C_1 represent the inductance and capacitance of low impedance stub, respectively. Also, the capacitance and inductance of radial stub are presented by C_2 and L_3, respectively. The EM and LC simulation results are indicated in Fig. 13(c). The values of LC model are computed and optimized using formulas outlined in [1]. Also, they are as follows: L_1=3.2, L_2=0.1, L_3=0.25, C_1=0.3 and C_2=2.08 (Units: C, pF; L, nH). The transfer function of Fig. 13(b) is calculated and presented in (1). Next, by equalling numerator of transfer function with zero, the equation of T_Z is achieved as (2). Notice, r is the matching impedance at input and output ports (r=50Ω). By altering the radius of the resonator, the position of T_z is shifted. For instance, by decreasing the R_1, T_Z moves to higher frequencies and the stopband width is limitted, illustrating an tuneable stopband. The effect of changes of R_1 is summarized in Table 1.

$$\frac{v_o}{v_i} = \frac{(2r(C_1C_2L_2L_3)S^4 + (L_2C_1 + L_2C_2 + L_3C_2)S^2 + 1))}{(C_1C_2L_3)(L_1(L_1 + 2L_2)S^5 + 2r(L_1 + L_2)S^4) + L_1(2C_2(L_2 + L_3) + C_1(L_1 + 2L_2))S^3 + a}, \quad (1)$$

where

$$a = C_2(L_1^{\,2} + r^2C_1L_3))S^3 + 2r(C_1(L_1 + L_2) + C_2(L_1 + L_2 + L_3))S^2 + (2L_1 + r^2C_1 + r^2C_2)S + 2r.$$

$$T_Z = \left| \frac{\sqrt{-\dfrac{C_1L_2 + C_2L_2 + C_2L_3 - \sqrt{(C_1L_2 + C_2L_2 + C_2L_3)^2 - 2C_1C_2L_2L_3}}{2C_1C_2L_2L_3}}}{2\pi} \right|. \quad (2)$$

Table 1 Variation of T_Z with different lengths of R_1

R_1 (mm)	C_3 (pF)	L_3 (nH)	Tz (GHz)
4.5	2.08	0.25	5.978
4	1.78	0.2	6.815
3.5	1.7	0.175	7.273
3	1.45	0.125	8.625

Fig. 14(a) shows the magnitude of S_{21}-parameter for the dual-band BPF as a function of different radius (R_1) of two big radial-stubs. As illustrated, the suppression level between first and second passbands is related to radius of two big radial-stubs. Therefore, the desirable suppression level will be realized by adjusting of this value. Fig. 14(b) illustrates the magnitude of S_{21}-parameter for the dual-band BPF as a function of different lengths of coupled feed lines (L_1). As can be seen, first and second passbands are related to lengths of feed lines. Thus, the ideal position of passbands for designer will be obtained using different lengths of these feed lines.

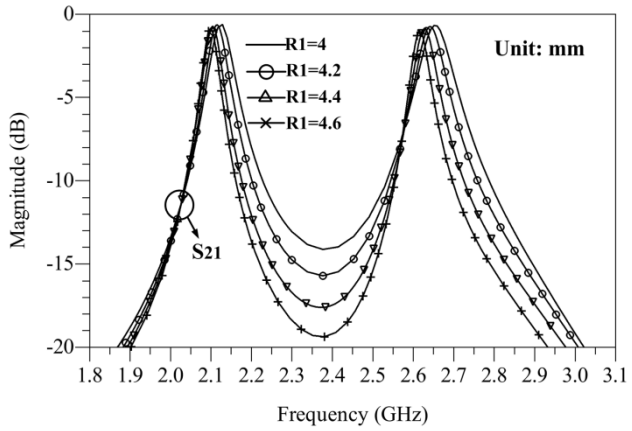

(a)

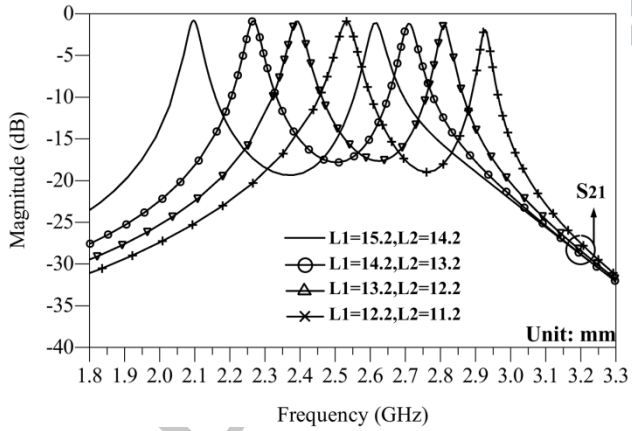

(b)

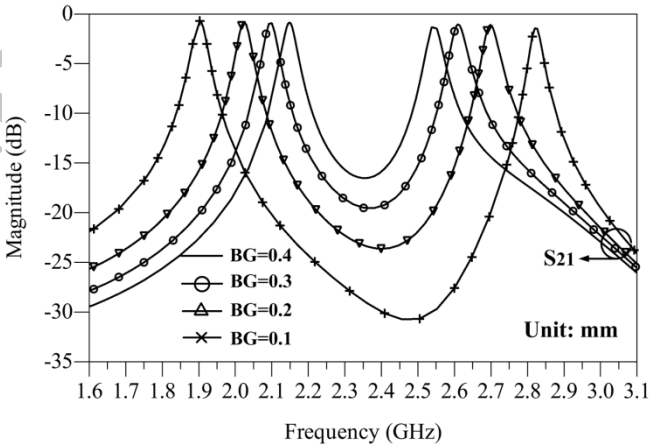

(c)

Fig. 14. The S_{21} parameter of dual-band BPF (a) As a function of different radius of two big radial-stubs (b) As a function of different lengths of coupled feed lines (c) As a function of different band-gaps.

Fig. 14(c) shows the magnitude of S_{21}-parameter for the BPF as a function of different band-gap distances. The central frequencies of first and second passbands are close together, whenever the width of band-gap is long. Similarly, the central frequencies of first and second passbands are far apart, whenever the width of band-gap is short. Thus, the desirable frequency distance between passbands (2.1 and 2.61 GHz) can be adjusted. The dimensions of dual-band BPF are: L_1=15.2, L_2=14.2, L_3=0.5 L_4=0.7, L_5=0.6, L_6=1.1, L_7=0.7, L_8=1.1, L_9=1.2, L_{10}=1.4, L_{11}=7.2, L_{12}=9.4, L_{13}=10, L_{14}=1.8, L_{15}=2, L_{16}=1.2, L_{17}=7.8, R_1=4.5, R_3=1.8, BG=0.3, BG_1=0.6 and BG_2=0.8 (all in millimeter).

3 SIMULATION AND MEASUREMENT RESULTS

The simulation results have been extracted using Advanced Design System (ADS 2011.10) software. The designed filters have been implemented on Rogers_RO4003 substrate (ε_r = 3.38, thickness = 0.508 mm and loss-tangent = 0.002) and they have been tested using a HP8757 network analyzer. Photograph of the manufactured filter, simulation and experimental results are illustrated in Fig. 15. The single-band BPF has a wide upper stopband up to 12.7 GHz with suppression level of -25 dB and the return loss of its passband is about -24 dB. For dual-band BPF, the return-losses are 16.8 and 15.9 dB in first and second passbands, respectively. Also, the rejection in stopband area is more than -20 dB up to 10 GHz. The operational frequencies of first and second passbands have been located at ~2.1 and ~2.6 GHz, corresponding to the 3G and 4G. The proposed circuits and some introduced papers in [2-34] are compared in Tables 2 and 3.

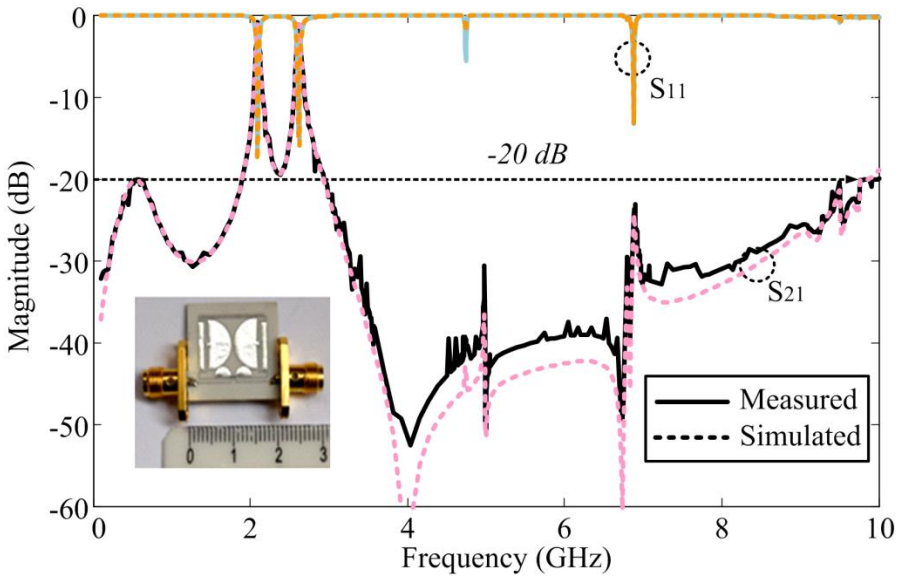

Fig. 15. Photograph of the manufactured filter, EM-simulation and measurement results of Dual-band BPF.

Table 2. Comparison among some reported works and dual-band BPF

Refs.	f (GHz)	FBW (%)	RL (dB)	IL (dB)	Size (λ_g^2)
[2]	3.5/5.24	-	14/15	1.52/1.65	1.51
[3]	1.9/4.85	28.4/11.1	20/23	1.69/2.44	0.012
[4]	2.49/3.49	15.6/8	11/25	1.2/1.2	-
[5]-BPFA	1.8/5.8	8.76/4.05	21/13	1.33/1.7	0.039
[5]-BPFB	2.4/5.8	4.63/3.6	17/15	1.35/1.97	0.097
[6]	1.57/2.45	9/8.5	17.5/22.6	1.26/2.4	0.01
[8]-BPF1	1.3/2.5	12.3/23.3	36/22	0.99/0.5	0.004
[8]-BPF2	1.21/2.48	26/10.3	20/25	0.6/0.43	0.0045
[9]	3.4/5.56	4.4/6.8	18/11	2.16/1.93	-
[10]	2.4/5.2	9.2/9.5	30/12	1.4/2.7	0.032
[22]	2.45/5.2	18/4.8	20/19	0.6/0.9	0.025
[25]	2.55/3.65	6.72/5.45	20/18	1.22/2.13	0.119
[36]	2.1/2.63	2.15/1.48	19.3/30.7	0.68/1.08	0.028
Dual-band BPF	**2.1/2.62**	**1.76/1.527**	16.8/15.9	**0.81/1.13**	0.028

Table 3. Comparison among some reported works and single-band BPF

Refs.	f (GHz)	FBW (%)	RL (dB)	IL (dB)	Size (λ_g^2)
[4]	2.48	11.2	11	1.2	-
[11]	1.5	-	15	1.2	0.0266
[12]	1.5	-	20	1.6	0.034
[18]	1	10	13	1.2	0.0288
[24]-BPF1	2.45	32	22	0.2	-
[24]-BPF2	2.8	23	26	0.2	-
[28]	8.4	7.9	25	1.53	0.042
[35]	2.79	1.64	20	0.9	0.024
Single-band BPF	**2.12**	**1.93**	**24**	**0.83**	**0.028**

4 CONCLUSION

Two compact BPFs using the coupled feed lines have been designed and tested. The miniaturized BPFs have wide stopband. By adopting the T-shaped open stubs and conventional rectangular suppressors on the coupled feed line, a single-band BPF is manufactured for 3G applications. To display an adjustable passband, the coupled feed lines combining with T-shaped open stubs using equivalent circuit are analyzed. In passband, the insertion loss and return loss are 0.83 and 24 dB, respectively. The unwanted frequencies in upper stopband are attenuated up to 12.7 GHz ($6f_c$) with -25 dB suppression level. In dual-band BPF, the performance of big radial resonator is analyzed using its transfer function to calculate the formula of transmission zero. Also, the central frequencies are 2.1 and 2.62 GHz, that it is suitable for 3G and 4G applications.

REFERENCES

[1] Hong, J.S.G. and Lancaster, M.J., 2004. *Microstrip filters for RF/microwave applications* (Vol. 167). John Wiley & Sons.

[2] Li P, Chu H, Zhao D, Chen RS. Compact Dual-Band Balanced SIW Bandpass Filter With Improved Common-Mode Suppression. IEEE Microwave and Wireless Components Letters. 2017;27(4):347-9.

[3] Du C, Ma K, Mou S. A Miniature SISL Dual-Band Bandpass Filter Using a Controllable Multimode Resonator. IEEE Microwave and Wireless Components Letters. 2017;27(6):557-9.

[4] Zhu H, Abbosh AM. Single-and dual-band bandpass filters using coupled stepped-impedance resonators with embedded coupled-lines. IEEE Microwave and Wireless Components Letters. 2016;26(9):675-7.

[5] Zhang ZC, Chu QX, Chen FC. Compact Dual-Band Bandpass Filters Using Open-/Short-Circuited Stub-Loaded λ/4 Resonators. IEEE Microwave and Wireless Components Letters. 2015;25(10):657-9.

[6] Peng Y, Zhang L, Fu J, Wang Y, Leng Y. Compact dual-band bandpass filter using coupled lines multimode resonator. IEEE Microwave and Wireless Components Letters. 2015;25(4):235-7.

[7] Wang S, Zhang D, Zhang Y, Qing L, Zhou D. Novel Dual-Mode Bandpass Filters Based on SIW Resonators under Different Boundaries. IEEE Microwave and Wireless Components Letters. 2017;27(1):28-30.

[8] Shen G, Che W, Feng W, Xue Q. Analytical design of compact dual-band filters using dual composite right-/left-handed resonators. IEEE Transactions on Microwave Theory and Techniques. 2017;65(3):804-14.

[9] Wang W, Cao Q, Yang C, Wang Y, Chen Y. Design of dual-bandpass filters using stepped-impedance circular ring resonator. Electronics Letters. 2015;51(25):2117-9.

[10] Xu LJ, Zhang G, Tang YM, Bo YM. Compact dual-mode dual-band bandpass filter with wide stopband for WLAN applications. Electronics Letters. 2015;51(17):1372-4.

[11] Li YL, Chen JX, Lu QY, Qin W, Li W, Bao ZH. A New and Simple Design Approach for Harmonic Suppression in Bandpass Filter. IEEE Microwave and Wireless Components Letters. 2017;27(2):126-8.

[12] Fernández-Prieto A, Bhatker J, Lujambio A, Martel J, Medina F, Boix RR. Balanced bandpass filter based on magnetically coupled coplanar waveguide folded-stepped impedance resonators. Electronics Letters. 2016;52(14):1229-31.

[13] Abbosh AM. Ultrawideband balanced bandpass filter. IEEE Microwave and Wireless Components Letters. 2011;21(9):480-2.

[14] Bagci F, Fernández-Prieto A, Lujambio A, Martel J, Bernal J, Medina F. Compact Balanced Dual-Band Bandpass Filter Based on Modified Coupled-Embedded Resonators. IEEE Microwave and Wireless Components Letters. 2017;27(1):31-3.

[15] Zhou WJ, Chen JX. High-selectivity tunable balanced bandpass filter with constant absolute bandwidth. IEEE Transactions on Circuits and Systems II: Express Briefs. 2017;64(8):917-21.

[16] Abbosh AM. Design method for ultra-wideband bandpass filter with wide stopband using parallel-coupled microstrip lines. IEEE Transactions on Microwave Theory and Techniques. 2012;60(1):31-8.

[17] Yang L, Choi WW, Tam KW, Zhu L. Novel Wideband Bandpass Filter with Dual Notched Bands Using Stub-Loaded Resonators. IEEE Microwave and Wireless Components Letters. 2017;27(1):25-7.

[18] Marín S, Martínez JD, Valero CI, Boria VE. Microstrip Filters With Enhanced Stopband Based on Lumped Bisected Pi-Sections With Parasitics. IEEE Microwave and Wireless Components Letters. 2017;27(1):19-21.

[19] Sun SJ, Su T, Deng K, Wu B, Liang CH. Compact microstrip dual-band bandpass filter using a novel stub-loaded quad-mode resonator. IEEE Microwave and Wireless Components Letters. 2013;23(9):465-7.

[20] Sun SJ, Wu B, Su T, Deng K, Liang CH. Wideband dual-mode microstrip filter using short-ended resonator with centrally loaded inductive stub. IEEE Transactions on Microwave Theory and Techniques. 2012;60(12):3667-73.

[21] Zhu H, Abbosh A. Compact tunable bandpass filter with wide tuning range of centre frequency and bandwidth using coupled lines and short-ended stubs. IET Microwaves, Antennas & Propagation. 2016;10(8):863-70.

[22] Liu H, Ren B, Guan X, Lei J, Li S. Compact dual-band bandpass filter using quadruple-mode square ring loaded resonator (SRLR). IEEE microwave and wireless components letters. 2013;23(4):181-3.

[23] Zhang S, Zhu L. Synthesis Design of Dual-Band Bandpass Filters With λ/4 Stepped-Impedance Resonators. IEEE Transactions on Microwave Theory and Techniques. 2013;61(5):1812-9.

[24] Marimuthu J, Bialkowski KS, Abbosh A. Compact bandpass filter with sharp passband and wide harmonic suppression using miniaturized coupled structure loaded with stepped-impedance stubs. Microwave and Optical Technology Letters. 2016;58(10):2505-8.

[25] Ieu W, Zhang D, Zhou D. High-selectivity dual-mode dual-band microstrip bandpass filter with multi-transmission zeros. Electronics Letters. 2017;53(7):482-4.

[26] Li YC, Wong H, Xue Q. Dual-mode dual-band bandpass filter based on a stub-loaded patch resonator. IEEE Microwave and Wireless Components Letters. 2011;21(10):525-7.

[27] Zhou K, Zhou CX, Wu W. Resonance Characteristics of Substrate-Integrated Rectangular Cavity and Their Applications to Dual-Band and Wide-Stopband Bandpass Filters Design. IEEE Transactions on Microwave Theory and Techniques. 2017;65(5):1511-24.

[28] Huang YM, Shao Z, Jiang W, Huang T, Wang G. Half-mode substrate integrated waveguide bandpass filter loaded with horizontal–asymmetrical stepped-impedance complementary split-ring resonators. Electronics Letters. 2016;52(12):1034-6.

[29] Xiao JK, Zhu M, Ma JG, Hong JS. Conductor-backed CPW bandpass filters with electromagnetic couplings. IEEE Microwave and Wireless Components Letters. 2016;26(6):401-3.

[30] Abbosh AM. Planar bandpass filters for ultra-wideband applications. IEEE Transactions on Microwave Theory and Techniques. 2007;55(10):2262-9.

[31] Hammed RT. Miniaturized dual-band bandpass filter using E-shape microstrip structure. AEU-International Journal of Electronics and Communications. 2015;69(11):1667-71.

[32] Xiao JK, Li Y, Zhang N, Ma JG. CPW bandpass filters with controllable passbands. AEU-International Journal of Electronics and Communications. 2016;70(8):1088-93.

[33] Huang L, Wu W, Zhang X, Lu H, Zhou Y, Yuan N. A novel compact and high performance bandpass filter based on SIW and CMRC technique. AEU-International Journal of Electronics and Communications. 2017;82:420-5.

[34] Sakotic Z, Crnojevic-Bengin V, Jankovic N. Compact circular-patch-based bandpass filter for ultra-wideband wireless communication systems. AEU-International Journal of Electronics and Communications. 2017;82:272-8.

[35] Ghaderi A, Roshani S. Microstrip bandpass filter with compact size for wireless communications, 1st National Conference of New Outlook on Electrical & Computer Engineering, Kermanshah, Iran. 2017.

[36] Ghaderi A, Golestanifar A, Shama F. Design of a compact microstrip tunable dual-band bandpass filter. AEU-International Journal of Electronics and Communications. 2017;82:391-6.